The Journal of Chemical Physics

Vibrational mode-specificity in the dynamics of the Cl + C_2H_6 → HCl + C_2H_5 reaction

Cite as: J. Chem. Phys. **155**, 114303 (2021); https://doi.org/10.1063/5.0062677
Submitted: 07 July 2021 . Accepted: 29 August 2021 . Published Online: 17 September 2021

Dóra Papp, Jun Li, Hua Guo, Gábor Czakó, et al.

The Journal of Chemical Physics ARTICLE scitation.org/journal/jcp

Vibrational mode-specificity in the dynamics of the Cl + C_2H_6 → HCl + C_2H_5 reaction

Cite as: J. Chem. Phys. 155, 114303 (2021); doi: 10.1063/5.0062677
Submitted: 7 July 2021 • Accepted: 29 August 2021 •
Published Online: 17 September 2021

Dóra Papp,[1,a] Jun Li,[2] Hua Guo,[3] and Gábor Czakó[1,a]

AFFILIATIONS

[1] MTA-SZTE Lendület Computational Reaction Dynamics Research Group, Interdisciplinary Excellence Centre and Department of Physical Chemistry and Materials Science, Institute of Chemistry, University of Szeged, Rerrich Béla tér 1, Szeged H-6720, Hungary

[2] School of Chemistry and Chemical Engineering and Chongqing Key Laboratory of Theoretical and Computational Chemistry, Chongqing University, Chongqing 401331, China

[3] Department of Chemistry and Chemical Biology, University of New Mexico, Albuquerque, New Mexico 87131, USA

[a] **Authors to whom correspondence should be addressed:** dorapapp@chem.u-szeged.hu and gczako@chem.u-szeged.hu

ABSTRACT

We report a detailed dynamics study on the mode-specificity of the Cl + C_2H_6 → HCl + C_2H_5 H-abstraction reaction. We perform quasi-classical trajectory simulations using a recently developed high-level *ab initio* full-dimensional potential energy surface by exciting five different vibrational modes of ethane at four collision energies. We find that all the studied vibrational excitations, except that of the CC-stretching mode, clearly promote the title reaction, and the vibrational enhancements are consistent with the predictions of the Sudden Vector Projection (SVP) model, with the largest effect caused by the CH-stretching excitations. Intramolecular vibrational redistribution is also monitored for the differently excited ethane molecule. Our results indicate that the mechanism of the reaction changes with increasing collision energy, with no mode-specificity at high energies. The initial translational energy mostly converts into product recoil, while a significant part of the excess vibrational energy remains in the ethyl radical. An interesting competition between translational and vibrational energies is observed for the HCl vibrational distribution: the effect of exciting the low-frequency ethane modes, having small SVP values, is suppressed by translational excitation, whereas a part of the excess vibrational energy pumped into the CH-stretching modes (larger SVP values) efficiently flows into the HCl vibration.

INTRODUCTION

Controlling the outcome of a chemical reaction has always been one of the main ambitions of chemists. In the 1970s, dynamics simulations on A + BC reactive systems started to investigate the effect of translational vs vibrational excitation on reactivity, and the results cumulated in what we call the Polanyi rules, some rules of thumb of chemical reaction dynamics.[1] The rules say that the position of the transition state (TS) along the reaction coordinate determines which form of energy is more efficient in promoting a chemical reaction: in the case of an early-barrier reaction, i.e., when the geometry of the reactant-like TS features a large A–B/C distance, translational excitation helps the system overcome the reaction barrier, whereas vibrational excitation enhances the reactivity of a late-barrier reaction, which has a product-like TS with an elongated B–C bond. The first step to larger, more complicated chemical systems was the investigation of the reactions of the water molecule with different atoms.[2–6] In the 1980s, Schatz and co-workers studied the mode- and bond-selectivity in such reactions by using quasi-classical trajectory (QCT) simulations and predicted that a five-quantum excitation of the OH stretching mode enhances the reactivity of the H + HOD → H_2 + OD reaction much more significantly than exciting the OD stretching reactant mode.[2] Later, experiments of the groups of Crim[3,5] and Zare[4] confirmed these predictions. At the end of the 1990s, Zhang and Light[6] performed the first quantum dynamics calculations on the H + HOD reaction: they studied the effect of mode-specific excitations on the ratio of the OD/OH products and obtained results in qualitative agreement with the experiment of Zare and co-workers.[4]

By the end of the 20th century, reaction dynamics has arrived at a stage where the investigation of the even more complex H-abstraction reactions of methane with atoms became possible.[7–9]

The dynamics of such polyatomic systems can be rather complicated and therefore hard to predict due to the growing number of the internal degrees of freedom (DOFs) and the coupling between them, which can also give rise to intramolecular vibrational redistribution (IVR),[10] especially when enough time is available. Accordingly, experiments of Liu and co-workers revealed interesting departures from the Polanyi rules in the case of the atom + methane reactions: (1) they showed that the excitation of the CH-stretching mode in the late-barrier Cl + CHD_3 reaction had no larger promoting effect than translational energy[11] and (2) CH-excitation in the F + CHD_3 reaction inhibited the cleavage of the C–H bond.[12] Furthermore, they also unraveled that the dominance of the OH + CD_3 product channel in the O + $CHD_3(v_1 = 1)$ reaction can be explained by the enlargement of the reactive cone of acceptance due to CH-stretching excitation.[13] These findings were later confirmed by reaction dynamics simulations on accurate *ab initio* analytical potential energy surfaces (PESs), made possible by pivotal fitting method developments.[14–18] Using these novel methods, Czakó and Bowman gave explanation to why vibrational energy has less effect than expected in activating the late-barrier Cl + CHD_3 reaction: they showed that deviations from the Polanyi rules are the most transparent at low collision energies, where van der Waals minima are allowed to guide the dynamics, whereas larger translational energy and therefore shorter reaction time drive the system to increasingly follow the traditional rules.[19–21] QCT simulations exploring mode-specificity on high-quality analytical PESs were performed for the F + CHD_3,[22,23] O + CH_4,[18] and the Br + CH_4[24] reactions as well. Furthermore, mode-specific reduced- and full-dimensional quantum dynamics calculations on atom + methane reactions were also carried out.[25–32]

Following the pioneering experimental and *ab initio* studies,[33–36] by the 2010s, the field of theoretical chemical reaction dynamics stepped to the next level by expanding toward complex reactive systems, including more than six atoms,[37,38] such as the investigation of the OH + CH_4 reaction by Li and Guo.[39] Later, the F/Cl/OH + CH_3OH reactions were also studied,[40–43] and a detailed mode-specific analysis was carried out for the F + CH_3OH reaction.[44] After experimental[45–48] and early direct dynamics and force-field-type PES-based investigations,[49–54] the first accurate nine-atomic full-dimensional spin–orbit-corrected analytical *ab initio* PES and the dynamics of the Cl + C_2H_6 → HCl + C_2H_5 reaction were reported in 2020 by two of the present authors (D.P. and G.C.), resolving a 25-year-old contradiction[55] between experiment and theory regarding the rotational distribution of the diatomic product.[56] Later, a similar PES was also developed by Papp and Czakó for the F + C_2H_6 reaction, allowing for accurate dynamics simulations, providing again excellent agreement with the experiment.[57]

While the Polanyi rules are still qualitatively applicable, their unambiguous extension for polyatomic reactions is not a straightforward task as the concept of an early/late barrier is difficult to generalize for different vibrational modes of the reactants. An alternative perspective is provided by the Sudden Vector Projection (SVP) model, developed by Jiang and Guo,[58,59] which has become an effective theoretical tool in predicting mode-specificity in direct reactions, i.e., when collision time is much shorter than that needed for the IVR. The SVP model is based on the assumption that the promoting effect of exciting a vibrational mode of the reactant molecule is proportional to the coupling between that mode and the reaction coordinate at the TS,[58] and it was successfully applied for many polyatomic reactive systems.[60–63]

The present study investigates the mode-specificity in a nine-atomic chemical reaction, namely, in the Cl + C_2H_6 → HCl + C_2H_5 hydrogen-abstraction reaction. By performing QCT simulations on a recently-developed accurate *ab initio* analytical PES,[56] we excite five different vibrational modes of the reactant ethane molecule and investigate the effect of these excitations on the reactivity compared to that of translational energy. We also follow the pre- and post-reaction distribution of energy during the reaction. SVP calculations are also carried out to predict the impact of vibrational/translational excitations. As discussed below, this reaction differs from other more activated H-abstraction reactions in that the zero-point energy (ZPE)-corrected reaction path has a submerged barrier and a shallow intermediate well. As a result, it is not obvious that mode-specificity exists.

COMPUTATIONAL DETAILS

Quasi-classical dynamics simulations are carried out at 1.0, 5.5, 10.0, and 20.0 kcal/mol collision energies for the $Cl(^2P_{3/2})$ + C_2H_6 → HCl + C_2H_5 reaction on a full-dimensional spin–orbit-corrected analytical *ab initio* PES constructed recently[56] using the Robosurfer program system designed for automated development of PESs based on permutationally invariant polynomial expansion.[64] The QCT simulations start either from the vibrational ground state of the reactant ethane molecule or by exciting one of five selected normal vibrational modes of ethane, each with one quantum. The effect of the excitation of the following normal modes of ethane is studied: ν_1—symmetric CH-stretching (8.54), ν_3—CC-stretching (2.74), ν_5—asymmetric CH-stretching (8.99), ν_6—CH_3 deformation (3.74), and ν_7—a degenerate CH-stretching mode (8.79), with fundamental harmonic energies obtained on the PES and given in kcal/mol in parentheses. These normal modes, along with the reaction coordinate at the TS structure, are illustrated in Fig. 1. The zero-point energy (ZPE) and the excitation of the different vibrational modes of ethane are set by standard normal-mode sampling at the beginning of the trajectories.[65]

The spatial orientation of the reactants is sampled randomly, and the initial distance between the Cl atom and the center of mass of the ethane molecule is $\sqrt{x^2 + b^2}$, where x = 16 bohr and the b impact parameter (the initial distance of the velocity vectors of the reactants) is varied between 0 and b_{max} (where the reaction probability vanishes) with a step size of 1.0 bohr. The trajectories are propagated with a 0.0726 fs time step until the largest atom–atom distance becomes larger than the largest initial one by 1 bohr. 500 trajectories are run at each b value for each collision energy and for each different excitation or the ground vibrational state of ethane.

To investigate IVR, we follow 100 QCTs for each of the above excitations and also for the ground vibrational state of ethane through 5000 time steps. The Cl atom is placed far so that the interaction between the reactants is negligible. We determine the mode-specific vibrational energies of ethane as detailed in Refs. 66 and 67 and plot them as a function of time t, integrated over the trajectories and the $(0, t)$ interval.

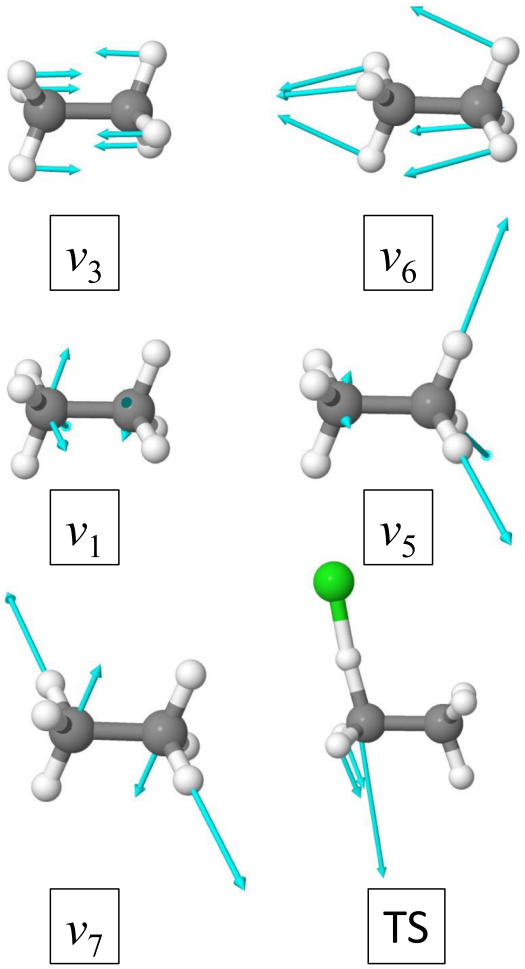

FIG. 1. Schematic representation of the normal-mode vibrations of ethane studied in the present QCT simulations and the reaction coordinate (imaginary mode) at the TS structure of the Cl + C_2H_6 → HCl + C_2H_5 reaction. For notations, see Table I.

Integral cross sections (ICSs) for the ground state and the excited reactions at each collision energy are calculated by using a b-weighted numerical integration of the opacity functions, *i.e.*, the $P(b)$ reaction probabilities as a function of the impact parameter b. For the products, we use different ZPE restrictions: (1) soft: the sum of the classical vibrational energy of the ethyl radical and the internal energy of the HCl product must be larger than the sum of the harmonic ZPE of C_2H_5 and the anharmonic ZPE of HCl corresponding to its actual rotational state (the variationally determined rovibrational energy levels of the HCl molecule are taken from Ref. 19), (2) hard: the previous constraints are set separately for each product, and (3) "ethyl": the restriction is only set for C_2H_5. The scattering angle distributions of the products are obtained by binning the cosine of the angle (θ) of the relative velocity vectors of the center of masses of the products and the reactants into five equidistant bins from −1 to 1, where $\cos(\theta) = -1$ ($\theta = 180^\circ$) corresponds to backward scattering. The rotational quantum number of HCl is obtained as detailed in Ref. 56, and the vibrational quantum number of HCl is determined by finding the variationally computed rovibrational energy level corresponding to the actual rotational state of HCl nearest to the classical internal energy of the HCl product.

Relative uncertainties of ICSs, product angular distributions, and opacity functions are tested against previous results[56] obtained for the ground state and the $v_1 = 1$ reactions by running 1000 trajectories with a 0.5 bohr step size in b and turn out to be always less than 10%; moreover, in the case of the non-constrained ICSs, the compared values do not differ more than 4%. Average (maximum) absolute deviations for the reaction probabilities and the hard-constrained HCl vibrational-state probabilities are 0.01 (0.04) and 0.03 (0.07), respectively.

In the framework of the SVP model, the overlaps, i.e., the SVP values, of the ethane vibrational modes with the reaction coordinate at the H-abstraction TS structure are calculated using the CCSD(T)-F12a/aug-cc-pVDZ optimized geometries and the normal-mode vectors of ethane when the Cl atom is placed far. These values are between 0 and 1, the two limits corresponding to weak and strong coupling with the reaction coordinate at the transition state, respectively.

RESULTS AND DISCUSSION

The mode-specific dynamics of the Cl($^2P_{3/2}$) + C_2H_6 → HCl + C_2H_5 H-abstraction reaction is investigated by performing QCT simulations on a high-quality full-dimensional *ab initio* analytical PES recently developed by two of the present authors.[56] The accuracy of the PES is highlighted by the 0.19 kcal/mol average deviation between the benchmark relative energies of the stationary points and those obtained on the PES, as shown in Fig. 2. The reaction features a 2.3 kcal/mol classical endothermicity, a

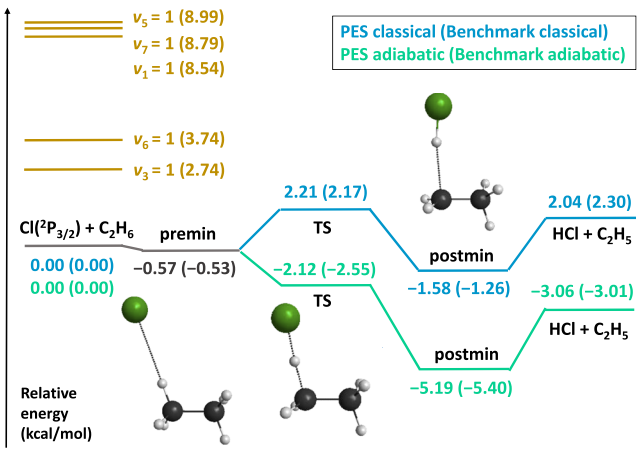

FIG. 2. Schematic potential energy surface of the Cl + C_2H_6 → HCl + C_2H_5 reaction comparing adiabatic (green) and classical (blue) relative energies obtained on the PES with benchmark (all-electron CCSDT(Q)/complete-basis-set-quality) data[68] in parentheses and showing vibrational energy levels of ethane, studied in the present QCT simulations, excited with one quantum (brown). Adapted from Papp *et al.*, J. Phys. Chem. Lett. **11**, 4762 (2020). Copyright 2020 Author(s), licensed under a Creative Commons Attribution 4.0 License.

classical barrier of 2.2 kcal/mol, and a −1.3 kcal/mol deep minimum in the exit channel with respect to the energy of the reactants. In contrast, if we take ZPE into account, the reaction becomes exothermic (−3.0 kcal/mol) and barrierless (the adiabatic relative energy of the TS is submerged below the reactants by 2.5 kcal/mol) with an exit channel minimum of −5.4 kcal/mol depth. A shallow pre-reaction minimum with a −0.5 kcal/mol depth is also identified from one-dimensional entrance channel scans.[56] The negative adiabatic barrier raises interesting questions regarding the Polanyi rules, since in such a reaction interaction time can be as effective in enhancing reactivity as translational or vibrational energy. In addition, the structure of the TS indicates only a slightly "late" barrier for the reaction.[56] To investigate the vibrational promoting effect, five different reactant vibrational [C–C stretching (ν_3), an asymmetric bending (ν_6), and the total-symmetric and two asymmetric C–H stretching] modes are excited with one quantum, for which the excitation energies are also shown in Fig. 2.

To be able to study the impact of vibrational excitation, one has to be aware of the magnitude of IVR, that is, how effectively the excess energy is kept within the selected mode. For this, we followed each mode-energy in a time range of 0–360 fs, while the time needed for collision in the QCT simulations varies in about a 150–650 fs scale, depending on the collision energy. It is worth mentioning that in single-collision experiments, collision time might be even longer. The results are shown in Fig. 3, where we can see that the two lowest-energy modes keep the excitation energy solidly, while the high-energy CH-stretching modes loose a great amount of energy in the first 180 fs. Thus, due to IVR, the predictions of the SVP model will certainly overestimate the effect of the CH-stretching excitations; however, in the case of higher collision energies, the SVP prognosis will be more realistic. Note that ZPE leakage, i.e., the mixing of the initial mode-energies corresponding to the ZPE of the reactant molecule between different normal modes, is a well-known issue of QCT simulations, whereas IVR is a realistic phenomenon usually well described by QCT. On the whole, despite IVR, the system has a clear mode-specific character after excitation, which can have significant impact on reactivity.

ICSs as a function of the total (initial translational + vibrational) and the collision (initial translational) energy, i.e., the excitation functions, of the title reaction for each reactant-mode excitation are shown in Fig. 4. We can see that reactivity decreases with increasing energy, which is not surprising for a barrierless exothermic reaction, where interaction time itself has a promoting effect. ICSs as a function of total energy (upper panel of Fig. 4) clearly show that the distribution of the same amount of energy between the vibrational and translational DOFs significantly alters reactivity. For example, when about 85%–90% of a total energy of 10 kcal/mol is in the vibrational DOF, i.e., in one of the C–H stretching modes, we can see almost a triple increase in reactivity (applying no ZPE constraints) with respect to the case when 100% of the total energy is fueled into the translational DOF ($v = 0$) and more than a double increase relative to when only 30%–40% of the total energy is in a vibrational mode (exciting ν_3 or ν_6 modes). This observation is fully consistent with the Polanyi rules in the case of this slightly late-barrier reaction. The stricter the ZPE constraint applied on the products is, the more apparent promoting effect of vibrational over translational energy we see: in the hard-restricted case, a vibrational enhancement factor of 16 is observed in the case of CH-stretching excitation

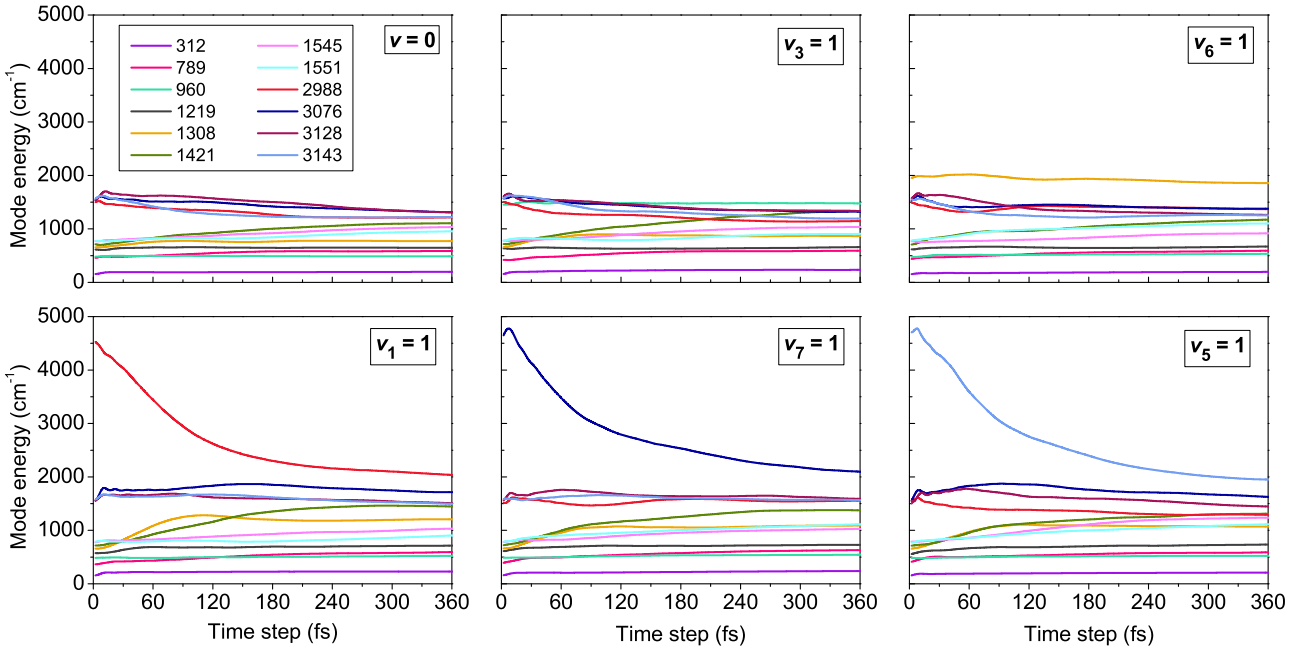

FIG. 3. Intramolecular vibrational-energy redistribution (IVR) followed in time for the ground vibrational state of ethane ($v = 0$) and also when five different ethane vibrational normal modes are excited with one quantum. Harmonic frequencies of ethane are given in cm^{-1}, and the corresponding modes are denoted with different colors.

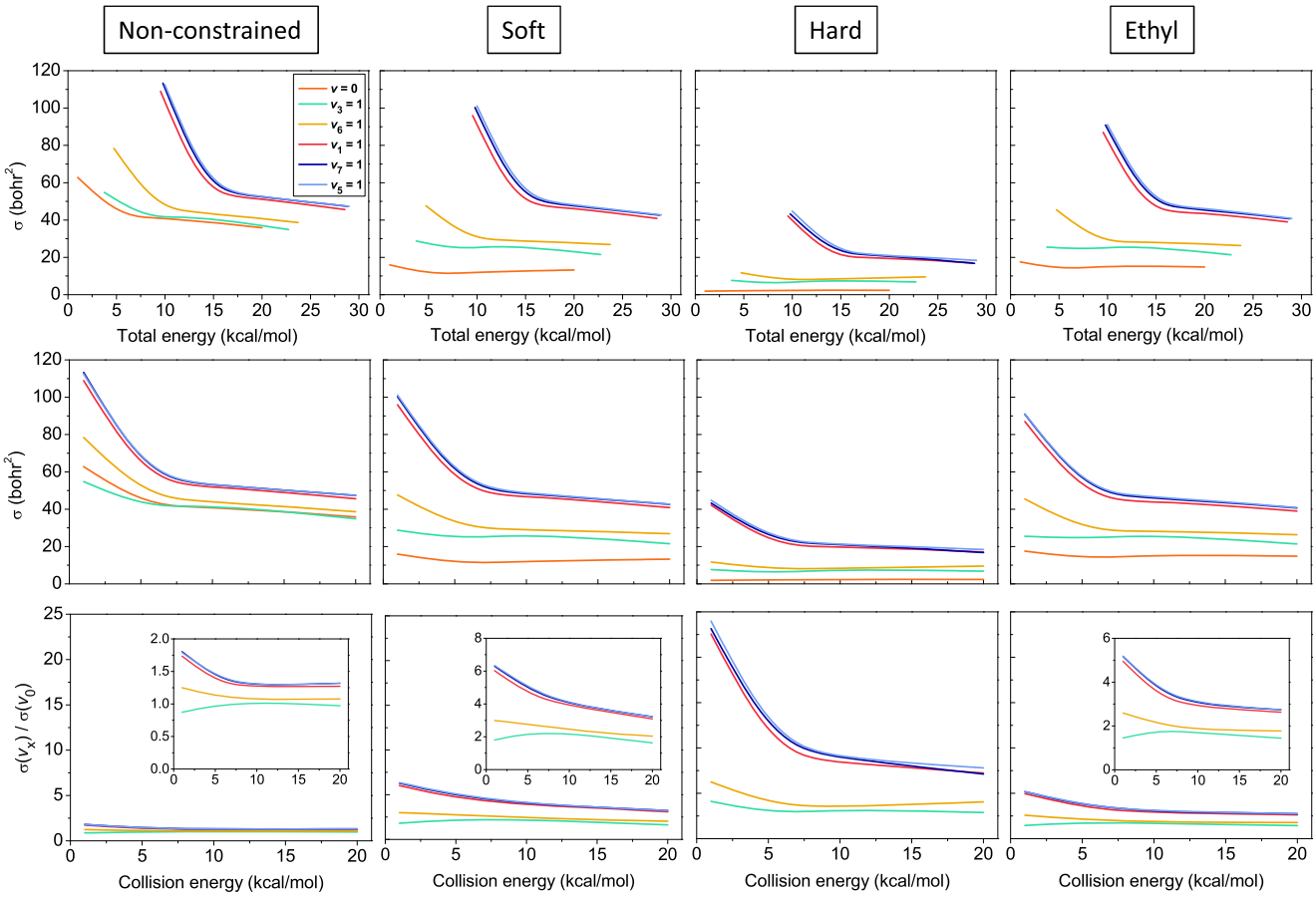

FIG. 4. Integral cross sections (ICSs) for the Cl + C_2H_6 → HCl + C_2H_5 reaction as a function of total energy (collision energy + vibrational excitation energy, upper panel) and collision energy (middle panel), as well as ratios of the ICSs of the Cl + $C_2H_6(v_x = 1)$ → HCl + C_2H_5 (x = 1, 3, 5, 6, 7) reactions with respect to the that of the Cl + $C_2H_6(v = 0)$ → HCl + C_2H_5 reaction as a function of collision energy (lower panel). The data are obtained with different ZPE constraints regarding the products: no-constraint (1st column), soft (2nd column), hard (3rd column), and only-ethyl (4th column). For further details, see the text.

relative to $v = 0$ and a four-times larger reactivity is seen relative to the excitation of the ν_3 and ν_6 modes at 10 kcal/mol total energy. As the total available energy increases, the promotion due to vibrational excitation becomes less marked because of the shorter interaction time, which, however, prevents IVR; thus, vibrational enhancement still remains substantial.

The considerable promoting effect of vibrational excitation, especially that of the CH-stretching modes, is also obvious when the ICSs are plotted as a function of the collision energy (middle row of Fig. 4), where an exact comparison of the effect of each mode can also be made at the collision energies employed (lowest panel of Fig. 4). The most pronounced enhancement, caused by the CH-stretching modes and resulting in a 25-times larger reactivity compared to $v = 0$ at the lowest collision energy, is observed when applying a hard ZPE constraint; however, even in the non-constrained case, a 25% increase in reactivity can be seen even for the ν_6 excitation. Taken together, we can claim that none of the above vibrational modes can be considered as spectators in the title reaction. The impact of vibrational excitation becomes less and less significant as collision energy increases since the shortened interaction time counteracts the overall reactivity. Interestingly, a different shape, featuring a maximum around 7–10 kcal/mol collision energy, can be seen for the enhancement curve corresponding to the CC-stretching-excited reaction; however, with hard ZPE restriction, it also adopts the decreasing shape observed for the other modes. Also somewhat surprisingly, in the case of the ν_6 deformation mode excitation, causing an overall near-constant enhancement in reactivity, a very shallow minimum emerges at around 10 kcal/mol collision energy in all the hard-constrained functions of Fig. 4.

The predictions of the SVP analysis are essentially consistent with the above dynamical observations; however, SVP might overestimate the effect of the excitations due to IVR, being most relevant at low collision energies. As we can see in Table I, the SVP values are quite high for the CH-stretching modes studied (ν_1, ν_5, ν_7), all near 0.3, which is clearly reflected in the calculated reactivity enhancement factors (lowest panel of Fig. 4), especially with the hard ZPE restriction, which at least partially eliminates the ZPE-leakage

TABLE I. Assignments, symmetries, harmonic frequencies, and SVP values of the reactant vibrational normal modes (and translation) for the $Cl + C_2H_6 \rightarrow HCl + C_2H_5$ reaction calculated at the UCCSD(T)-F12a/aug-cc-pVDZ level of theory. The SVP values for degenerate modes are the averages of the two components.

Assignments	Symmetry	No.	Freq. (cm^{-1})	SVP values
Torsion	A_{1u}	ν_4	311	0.001
CH_3 rock.	E_u	ν_{12}	822	0.154
CC str.	A_{1g}	ν_3	1015	0.034
CH_3 rock.	E_g	ν_9	1223	0.117
CH_3 s-deform.	A_{2u}	ν_6	1406	0.041
CH_3 s-deform.	A_{1g}	ν_2	1426	0.052
CH_3 d-deform.	E_g	ν_8	1506	0.064
CH_3 d-deform.	E_u	ν_{11}	1507	0.066
CH_3 s-str.	A_{1g}	ν_1	3035	0.353
CH_3 s-str.	A_{2u}	ν_5	3035	0.323
CH_3 d-str.	E_g	ν_7	3096	0.294
CH_3 d-str.	E_u	ν_{10}	3119	0.385
Translation				0.091

error of QCT. However, somewhat contrary to the SVP predictions (ν_1, ν_5, ν_7—overlaps in decreasing order), QCT shows the excitation of the ν_5 CH-stretching as the most effective, followed by ν_7 and ν_1, even if only very slight differences can be observed in the excitation functions. The two low-frequency vibrational modes studied here, the CC-stretching (ν_3) and the CH_3 deformations (ν_6), are predicted to be much less effective in promoting the reaction by SVP, also consistent with the QCT results. SVP gives a slightly higher value (0.041) for the ν_6 mode compared to CC-stretching (0.034), and accordingly, in Fig. 4, we usually see a larger enhancement in the case of ν_6 excitation with respect to ν_3, with the largest difference at the lowest collision energy. Beyond the vibrational modes investigated in this work, SVP suggests that exciting the ν_9 and ν_{12} CH_3 rocking modes of ethane can also have a considerable boosting effect on reactivity, and the ν_{10} excitation is predicted to be even slightly more efficient in increasing reactivity than the other CH-stretching modes. On the contrary, SVP indicates that, e.g., the ν_4 torsional mode is expected to act as a spectator during the reaction.

Probabilities of the title reaction in the case of different ethane excitations as a function of the b impact parameter, i.e., the opacity functions, obtained from the QCT simulations at each collision energy are plotted in the upmost panel of Fig. 5. The largest maximum impact parameter values (b_{max}), where the reaction probability vanishes, are observed at the lowest collision energy for all types of excitations, which underlies the above conclusion concerning the promoting effect of reaction time: slowly moving reactants can be attracted to each other by dispersion interactions from as far as 13 bohr. At higher energies, the b_{max} value loses its collision-energy dependence: it is 8 bohr in almost every case; however, larger impact parameters contribute increasingly to reactivity with increasing translational excitation. Promotion of the reaction caused by the CH-stretching mode excitations is also apparent from the opacity functions. At small b values, the reaction probabilities are not very different at the two lowest collision energies; thus, the drastic decrease in the ICS values between these two energies (Fig. 4) is mostly originated from the much smaller b_{max} values. The drop in b_{max} seems to have the greatest effect on the reaction promotion induced by the CH-stretching excitations, which endures the most notable decrease between the two lowest collision energies (lowest panel of Fig. 4). We can also observe that neither the shape of the opacity functions nor the b_{max} value features any mode-specific character. Opacity functions along with the product scattering angle distributions, which are depicted in the 2nd row of Fig. 5 and become more and more forward-scattered as collision energy increases without showing dependence on the particular ethane mode excitation (except the minor effects at the lowest collision energy), indicate an indirect mechanism at low energies and an increasingly dominant stripping mechanism at higher energies. During the latter, the fast Cl atom strips away a H atom from the ethane molecule while keeping its initial direction. Interestingly, we can observe a slight inhibiting effect of the CC-stretching excitation in the reaction probabilities, especially at 1 kcal/mol collision energy, which is also reflected in the integral cross sections of Fig. 4 (non-constrained case).

The post-reaction distribution of energy, providing an insight into the pace of the dynamics, is also investigated (see the two lower panels of Fig. 5). Internal energy distributions of the ethyl radical product show only a slight dependence on collision energy (widen, flatten, and blue-shift with increasing energy) but are clearly dependent on which ethane mode is excited. Their maxima shift toward larger internal energies, with a significant part of the corresponding vibrational excitation energy. In contrast, the relative translational energy distributions of the products do not show any mode-specificity; on the other hand, with increasing collision energy, they become wider with blue-shifting maxima. Such a post-reaction distribution of energy indicates that an increasingly direct dynamics evolves with increasing translational excitation: the products can more and more easily separate because most of the collision energy is transferred into their relative transitional motion. At the same time, the vibrational excitation energy given to ethane is seen to be mostly remaining in the internal DOFs of the ethyl radical. From the internal energy distributions, it is apparent that a substantial part of the trajectories is ZPE-violating.

To investigate the effect of ZPE restrictions, in Fig. 6, we plot the same dynamics properties as shown in Fig. 5, but with soft and hard ZPE constraints applied at the lowest collision energy, where the largest effects can be expected. Since the "ethyl" constraint gives very similar results for the ICSs as the soft restriction, as seen in Fig. 4, we omit that constraint from further discussion. As shown in Fig. 6, the soft ZPE restriction mainly affects the probabilities of the ground state and the $\nu_{3,6} = 1$ excited reactions and does not have a significant effect on the product angular and the internal energy distributions. However, the soft-constrained relative translational energy distributions, besides showing a faster decay relative to the non-constrained ones, develop some mode-specificity as well, and the most pronounced ZPE effect is seen in the case of the $\nu = 0$ reaction, where the distribution loses its Gaussian shape. The hard ZPE restriction has a larger effect than the soft constraint, making the reaction probabilities drop significantly, especially for the unexcited and the $\nu_{3,6} = 1$ reactions, where the b_{max} values also decrease. Nevertheless, like the soft case, the hard restriction provides similar angular distributions as the non-restricted analysis. The cut in the

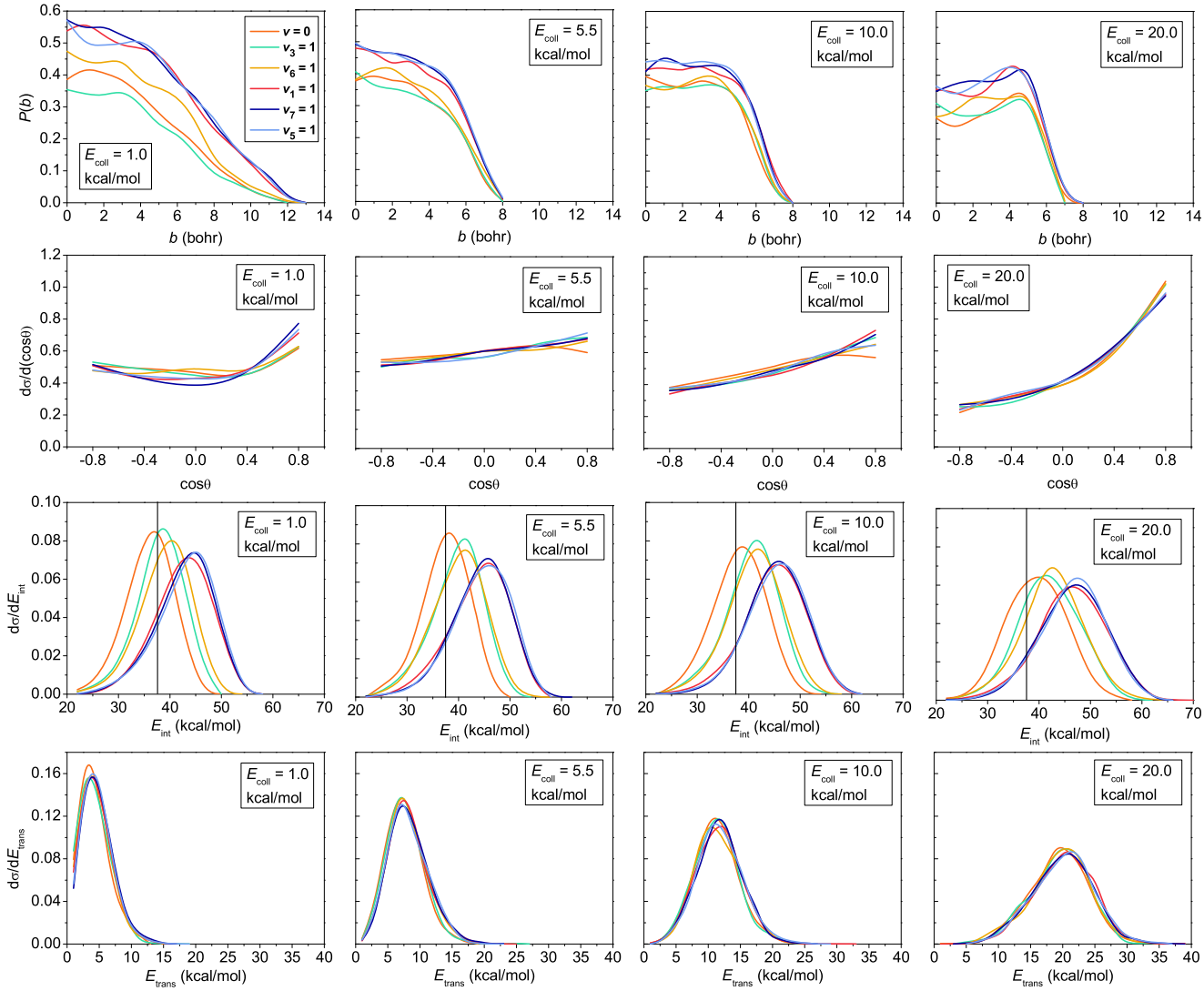

FIG. 5. Opacity functions (upmost panel), normalized product scattering angle distributions (upper middle panel), normalized internal energy distributions of the ethyl radical product (lower middle panel, where the black lines refer to the ZPE of the ethyl radical, 37.4 kcal/mol), and normalized product relative translational energy distributions (lowest panel) of the Cl + $C_2H_6(v = 0) \rightarrow$ HCl + C_2H_5 and Cl + $C_2H_6(v_x = 1) \rightarrow$ HCl + C_2H_5 (x = 1, 3, 5, 6, 7) reactions at 1.0, 5.5, 10.0, and 20.0 kcal/mol collision energies.

hard-constrained internal energy distribution of the ethyl radical at its ZPE is, of course, not surprising, and the translational energy distributions of the products also feature a much faster decay relative to the non-restricted case, most noticeably for the unexcited reaction, and mode-specificity also emerges.

The initial translational and the excess vibrational energy can flow not only into the internal DOFs of the ethyl radical but, of course, also into those of the HCl product. In Fig. 7, we show the relative populations of the v_{HCl} = 0, 1, and 2 vibrational states of the HCl molecule in the case of different ethane vibrational excitations and collision energies. (Since the contribution of the rotational energy of HCl is a very small fraction of the total energy, here we only focus on the vibration of HCl.)[56] In the reaction of unexcited ethane at the lowest collision energy, all the HCl molecules are formed in their ground vibrational state since the total energy (1.00 kcal/mol collision energy and 3.01 kcal/mol reaction energy released) is below the 4.29 kcal/mol threshold to reach the v_{HCl} = 1 state. As collision energy increases, the v_{HCl} = 1 state becomes more and more populated in the case of the vibrationally unexcited reaction, and a similar effect is also seen when the CC-stretching and the CH_3-deformation modes are excited in ethane. In contrast, when the excess vibrational energy is pumped into the CH-stretching modes, a considerable amount of energy flows into the HCl vibration, which is not surprising, since these modes have the largest SVP values,

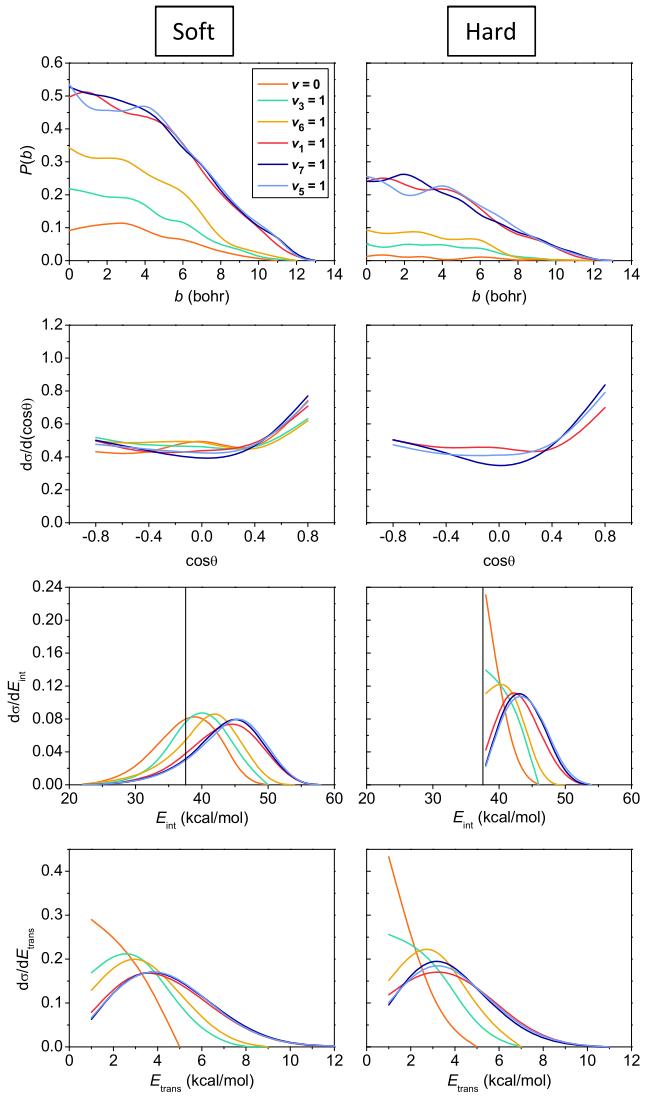

FIG. 6. Soft- and hard-ZPE-constrained opacity functions (upmost panel), normalized product scattering angle distributions (upper middle panel), normalized internal energy distributions of the ethyl radical product (lower middle panel, where the black lines refer to the ZPE of the ethyl radical, 37.4 kcal/mol), and normalized product relative translational energy distributions (lowest panel) of the Cl + C_2H_6(v = 0) → HCl + C_2H_5 and Cl + C_2H_6(v_x = 1) → HCl + C_2H_5 (x = 1, 3, 5, 6, 7) reactions at 1.0 kcal/mol collision energy. Note that due to the low hard-constrained reaction probabilities for the v = 0 and $v_{3,6}$ = 1 cases, their angular distributions are not plotted.

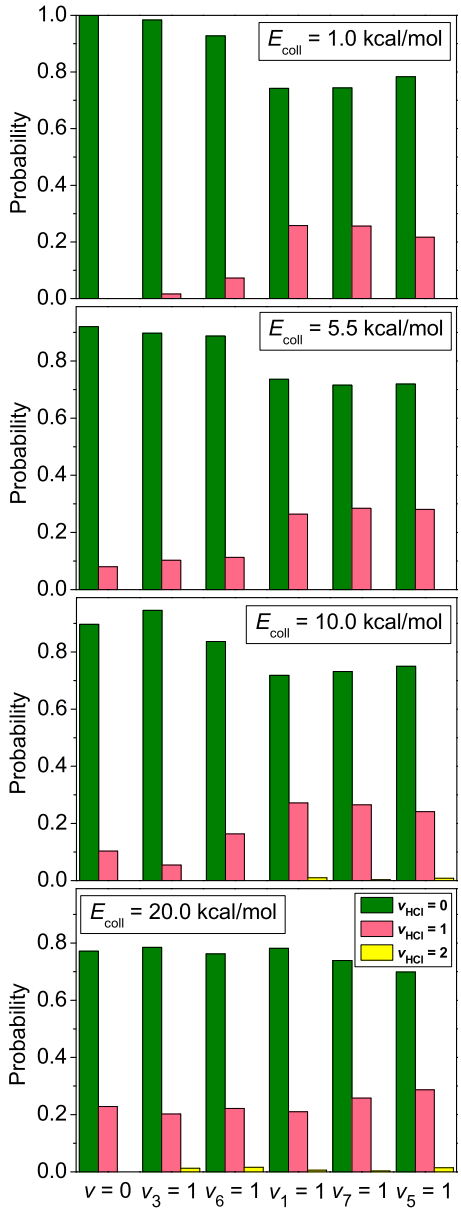

FIG. 7. Vibrational-state distributions of the HCl product of the Cl + C_2H_6(v = 0) → HCl(v_{HCl}) + C_2H_5 and Cl + C_2H_6(v_x = 1) → HCl(v_{HCl}) + C_2H_5 (x = 1, 3, 5, 6, 7) reactions at 1.0, 5.5, 10.0, and 20.0 kcal/mol collision energies obtained with hard ZPE restriction. (Note that in the 20.0 kcal/mol case, a v_{HCl} = 3 probability of 0.2% also appears in the case of exciting the v_1 mode.)

i.e., overlaps with the reaction coordinate at the TS. However, this effect could be counterbalanced by the increasing collision energy, because in a more direct reaction, there is less time for complex-forming and thus less possibility to such an energy redistribution. Accordingly, Fig. 7 shows only slight changes in the v_{HCl} = 0/v_{HCl} = 1 ratio in the case of the CH-stretching excitations at the different collision energies. Moreover, for the largest collision energy, this ratio becomes quite similar for all types of excitations and the unexcited reaction as well. Thus, it seems that a competition can be observed between translational and vibrational energies for the HCl vibrational excitation: when exciting the ν_3 and ν_6 modes, which have small SVP overlaps (0.03–0.04), not only the excess vibrational but also an increasing part of the initial translational energy is converted into HCl vibration (the SVP value for the translational mode is 0.09), whereas if the CH-stretching modes (having SVP values near 0.3) are excited, a significant portion of the excess vibrational energy

will flow into the HCl vibration, while translational excitation does not really affect the vibrational state of HCl in this case. At 10 and 20 kcal/mol collision energies, where the total available energy exceeds the 20.68 kcal/mol threshold needed for the $v_{HCl} = 2$ state, it also appears (except for the unexcited reaction at 20 kcal/mol), however, with very low population.

CONCLUSIONS

In the present work, we investigate the vibrational mode-specificity in a nine-atomic, namely, the $Cl + C_2H_6 \rightarrow HCl + C_2H_5$, reaction. We perform QCT simulations using a recently developed high-level full-dimensional *ab initio* PES and excite five different vibrational modes of ethane (ν_1—symmetric CH-stretching, ν_3—CC-stretching, ν_5—asymmetric CH-stretching, ν_6—CH_3 deformation, and ν_7—degenerate CH-stretching), each with one quantum, at four collision energies. We study the competing effects of vibrational and translational excitation on reactivity, on the post-reaction distribution of energy, and on the reaction mechanism, as well. To study the validity of the extended Polanyi rules, after determining the possible magnitude of IVR, we also compare our results with the predictions of the SVP model, where we see an excellent general agreement. We find that the mechanism of the title reaction is basically independent of vibrational excitation but changes with collision energy: at higher energies, the stripping mechanism becomes dominant over the indirect pathways, the latter mostly observed at low energies. The initial translational energy mainly converts into product recoil no matter which reactant mode is excited; however, applying different ZPE constraints introduces some artificial mode dependency into the product translational energy distribution, while the internal energy distribution of the ethyl radical features substantial mode-specificity, but is practically independent of translational excitation. The majority of the excess vibrational energy remains in the ethyl radical; however, for the HCl vibration, a competing behavior of vibrational and translational excitation is observed: the effect of increasing collision energy overcomes that of the excitation of the two low-frequency modes of ethane, whereas when the CH-stretching modes are excited, a part of the excess vibrational energy is efficiently driven to HCl vibration. This observation is in accordance with the SVP results, predicting overlaps 0.03–0.04, 0.09, and 0.29–0.35, respectively, for the above low-frequency, translational, and CH-stretching modes. On the whole, all the vibrational modes, whose effect is studied here in detail, except ν_3, clearly promote the reaction, and the enhancement due to CH-stretching excitations can reach even a factor of 25 at low collision energies. These vibrational excitations represent, of course, non-local motion; however, more local vibrational enhancement effects can also be studied in the future by replacing one or more hydrogen atoms of ethane with deuterium. We hope that our work will also motivate detailed experimental investigations on the vibrational mode-specificity of the title reaction.

ACKNOWLEDGMENTS

G.C. and D.P. acknowledge the financial support from the National Research, Development and Innovation Office–NKFIH, K-125317; the Ministry of Human Capacities, Hungary, under Grant No. 20391-3/2018/FEKUSTRAT; and the Momentum (Lendület) Program of the Hungarian Academy of Sciences. G.C. and D.P. also thank Viktor Tajti for performing the IVR computations. J.L. acknowledges the support from the Chongqing Municipal Natural Science Foundation (Grant No. cstc2019jcyj-msxmX0087). H.G. was supported by the Department of Energy (Grant No. DE-SC0015997) and acknowledges the Alexander von Humboldt Foundation for a Humboldt Research Award.

The authors have no conflicts to disclose.

DATA AVAILABILITY

The data that support the findings of this study are available from the corresponding authors upon reasonable request.

REFERENCES

[1] J. C. Polanyi, Science **236**, 680 (1987).
[2] G. C. Schatz, M. C. Colton, and J. L. Grant, J. Phys. Chem. **88**, 2971 (1984).
[3] A. Sinha, M. C. Hsiao, and F. F. Crim, J. Chem. Phys. **92**, 6333 (1990).
[4] M. J. Bronikowski, W. R. Simpson, B. Girard, and R. N. Zare, J. Chem. Phys. **95**, 8647 (1991).
[5] R. B. Metz, J. D. Thoemke, J. M. Pfeiffer, and F. F. Crim, J. Chem. Phys. **99**, 1744 (1993).
[6] D. H. Zhang and J. C. Light, J. Chem. Soc., Faraday Trans. **93**, 691 (1997).
[7] W. R. Simpson, A. J. Orr-Ewing, and R. N. Zare, Chem. Phys. Lett. **212**, 163 (1993).
[8] W. R. Simpson, T. P. Rakitzis, S. A. Kandel, A. J. Orr-Ewing, and R. N. Zare, J. Chem. Phys. **103**, 7313 (1995).
[9] A. J. Orr-Ewing, W. R. Simpson, T. P. Rakitzis, S. A. Kandel, and R. N. Zare, J. Chem. Phys. **106**, 5961 (1997).
[10] D. J. Nesbitt and R. W. Field, J. Phys. Chem. **100**, 12735 (1996).
[11] S. Yan, Y.-T. Wu, B. Zhang, X.-F. Yue, and K. Liu, Science **316**, 1723 (2007).
[12] W. Zhang, H. Kawamata, and K. Liu, Science **325**, 303 (2009).
[13] F. Wang and K. Liu, Chem. Sci. **1**, 126 (2010).
[14] B. J. Braams and J. M. Bowman, Int. Rev. Phys. Chem. **28**, 577 (2009).
[15] G. Czakó, B. C. Shepler, B. J. Braams, and J. M. Bowman, J. Chem. Phys. **130**, 084301 (2009).
[16] G. Czakó and J. M. Bowman, Proc. Natl. Acad. Sci. U.S.A. **109**, 7997 (2012).
[17] G. Czakó, R. Liu, M. Yang, J. M. Bowman, and H. Guo, J. Phys. Chem. A **117**, 6409 (2013).
[18] R. Liu, M. Yang, G. Czakó, J. M. Bowman, J. Li, and H. Guo, J. Phys. Chem. Lett. **3**, 3776 (2012).
[19] G. Czakó and J. M. Bowman, Science **334**, 343 (2011).
[20] G. Czakó and J. M. Bowman, J. Chem. Phys. **136**, 044307 (2012).
[21] Z. Zhang, Y. Zhou, D. H. Zhang, G. Czakó, and J. M. Bowman, J. Phys. Chem. Lett. **3**, 3416 (2012).
[22] G. Czakó and J. M. Bowman, J. Am. Chem. Soc. **131**, 17534 (2009).
[23] J. Palma and U. Manthe, J. Chem. Phys. **146**, 214117 (2017).
[24] G. Czakó, J. Chem. Phys. **138**, 134301 (2013).
[25] R. Welsch and U. Manthe, J. Chem. Phys. **141**, 051102 (2014).
[26] T. Westermann, J. B. Kim, M. L. Weichman, C. Hock, T. I. Yacovitch, J. Palma, D. M. Neumark, and U. Manthe, Angew. Chem., Int. Ed. Engl. **53**, 1122 (2014).
[27] J. Qi, H. Song, M. Yang, J. Palma, U. Manthe, and H. Guo, J. Chem. Phys. **144**, 171101 (2016).
[28] F. Meng, W. Yan, and D. Wang, Phys. Chem. Chem. Phys. **14**, 13656 (2012).
[29] W. Yan, F. Meng, and D. Wang, J. Phys. Chem. A **117**, 12236 (2013).
[30] W. Yan and D. Wang, Chem. Phys. Lett. **603**, 41 (2014).
[31] N. Liu and M. Yang, J. Chem. Phys. **143**, 134305 (2015).
[32] B. Fu, X. Shan, D. H. Zhang, and D. C. Clary, Chem. Soc. Rev. **46**, 7625 (2017).
[33] J. T. Jodkowski, M.-T. Rayez, J.-C. Rayez, T. Bérces, and S. Dóbé, J. Phys. Chem. A **102**, 9230 (1998).
[34] S. Rudić, C. Murray, D. Ascenzi, H. Anderson, J. N. Harvey, and A. J. Orr-Ewing, J. Chem. Phys. **117**, 5692 (2002).
[35] S. Rudić, C. Murray, J. N. Harvey, and A. J. Orr-Ewing, Phys. Chem. Chem. Phys. **5**, 1205 (2003).

[36]C. Murray, A. J. Orr-Ewing, R. L. Toomes, and T. N. Kitsopoulos, J. Chem. Phys. **120**, 2230 (2004).
[37]G. Czakó, T. Győri, D. Papp, V. Tajti, and D. A. Tasi, J. Phys. Chem. A **125**, 2385 (2021).
[38]J. Li, B. Zhao, D. Xie, and H. Guo, J. Phys. Chem. Lett. **11**, 8844 (2020).
[39]J. Li and H. Guo, J. Chem. Phys. **143**, 221103 (2015).
[40]M. L. Weichman, J. A. DeVine, M. C. Babin, J. Li, L. Guo, J. Ma, H. Guo, and D. M. Neumark, Nat. Chem. **9**, 950 (2017).
[41]D. Lu, J. Li, and H. Guo, CCS Chem. **2**, 882 (2020).
[42]O. Roncero, A. Zanchet, and A. Aguado, Phys. Chem. Chem. Phys. **20**, 25951 (2018).
[43]D. Lu, J. Behler, and J. Li, J. Phys. Chem. A **124**, 5737 (2020).
[44]D. Lu and J. Li, Theor. Chem. Acc. **139**, 157 (2020).
[45]S. A. Kandel, T. P. Rakitzis, T. Lev-On, and R. N. Zare, J. Chem. Phys. **105**, 7550 (1996).
[46]S. A. Kandel, T. P. Rakitzis, T. Lev-On, and R. N. Zare, Chem. Phys. Lett. **265**, 121 (1997).
[47]S. Rudić, D. Ascenzi, and A. J. Orr-Ewing, Chem. Phys. Lett. **332**, 487 (2000).
[48]C. Huang, W. Li, and A. G. Suits, J. Chem. Phys. **125**, 133107 (2006).
[49]S. Rudić, C. Murray, J. N. Harvey, and A. J. Orr-Ewing, J. Chem. Phys. **120**, 186 (2004).
[50]S. J. Greaves, J. Kim, A. J. Orr-Ewing, and D. Troya, Chem. Phys. Lett. **441**, 171 (2007).
[51]S. J. Greaves, A. J. Orr-Ewing, and D. Troya, J. Phys. Chem. A **112**, 9387 (2008).
[52]C. Rangel and J. Espinosa-Garcia, Phys. Chem. Chem. Phys. **20**, 3925 (2018).
[53]J. Espinosa-Garcia, E. Martinez-Nuñez, and C. Rangel, J. Phys. Chem. A **122**, 2626 (2018).
[54]J. C. Corchado, M. G. Chamorro, C. Rangel, and J. Espinosa-Garcia, Theor. Chem. Acc. **138**, 26 (2019).
[55]T. P. Rakitzis, Science **371**, 886 (2021).
[56]D. Papp, V. Tajti, T. Győri, and G. Czakó, J. Phys. Chem. Lett. **11**, 4762 (2020).
[57]D. Papp and G. Czakó, J. Chem. Phys. **153**, 064305 (2020).
[58]B. Jiang and H. Guo, J. Chem. Phys. **138**, 234104 (2013).
[59]H. Guo and B. Jiang, Acc. Chem. Res. **47**, 3679 (2014).
[60]B. Jiang and H. Guo, J. Am. Chem. Soc. **135**, 15251 (2013).
[61]J. Li and H. Guo, J. Phys. Chem. A **118**, 2419 (2014).
[62]H. Guo and K. Liu, Chem. Sci. **7**, 3992 (2016).
[63]M. Stei, E. Carrascosa, A. Dörfler, J. Meyer, B. Olasz, G. Czakó, A. Li, H. Guo, and R. Wester, Sci. Adv. **4**, eaas9544 (2018).
[64]T. Győri and G. Czakó, J. Chem. Theory Comput. **16**, 51 (2020).
[65]W. L. Hase, *Encyclopedia of Computational Chemistry* (Wiley, New York, 1998), pp. 399–407.
[66]G. Czakó, J. Phys. Chem. A **116**, 7467 (2012).
[67]I. Szabó and G. Czakó, J. Chem. Phys. **145**, 134303 (2016).
[68]D. Papp, B. Gruber, and G. Czakó, Phys. Chem. Chem. Phys. **21**, 396 (2019).